International Journal of Heat and Fluid Flow 30 (2009) 266–275

Contents lists available at ScienceDirect

International Journal of Heat and Fluid Flow

journal homepage: www.elsevier.com/locate/ijhff

Turbulence measurements in the inlet plane of a centrifugal compressor vaneless diffuser

Ali Pinarbasi *

Department of Mechanical Engineering, Engineering Faculty, Cumhuriyet University, 58140 Sivas, Turkey

ARTICLE INFO

Article history:
Received 24 April 2008
Received in revised form 3 December 2008
Accepted 4 December 2008
Available online 12 January 2009

Keywords:
Turbulence measurements
Diffuser flow
Vaneless
Compressor

ABSTRACT

Detailed flow measurements at the inlet of a centrifugal compressor vaneless diffuser are presented. The mean 3-d velocities and six Reynolds stress components tensor are used to determine the turbulence production terms which lead to total pressure loss. High levels of turbulence kinetic energy were observed in both the blade and passage wakes, but these were only associated with high Reynolds stresses in the blade wakes. For this reason the blade wakes mixed out rapidly, whereas the passage wake maintained its size, but was redistributed across the full length of the shroud wall. Peak levels of Reynolds stress occurred in regions of high velocity shear and streamline curvature which would tend to destabilize the shear gradient. Four regions in the flow are identified as potential sources of loss - the blade wake, the shear layers between passage wake and jet, the thickened hub boundary layer and the interaction region between the secondary flow within the blade wake and the passage vortex. The blade wakes generate most turbulence, with smaller contributions from the hub boundary layer and secondary flows, but no significant contribution is apparent from the passage wake shear layers.

1. Introduction

The overall efficiency of a centrifugal compressor is equally dependent on the good design of both impeller and diffuser. At the impeller inlet, the flow is uniform but at the impeller outlet the flow is highly distorted and three-dimensional due to strong secondary flows and mixing within the impeller. A major objective of the turbomachinery designer is to minimize the aerodynamic losses which result both within the turbomachine blade passages and downstream as non-uniformities in the flow are mixed out. Such impeller exit flows have been measured by Dean and Senoo (1960), Krain (1988), Maksoud and Johnson (1989) and Farge and Johnson (1992).

The mixing out of this highly distorted and 3-d flow in the diffuser has been observed by previous researchers (Inoue and Cumpsty, 1984; Senoo and Ishida, 1975; Pinarbasi and Johnson, 1994; Hagelstein et al., 2000; Hillewaert and Van den Braembussche, 1999; Shum et al., 2000). The blade wakes were observed to mix out rapidly, while the passage wake, which is located on the shroud side of the passage, mixes out slowly. At the diffuser exit, a Hele–Shaw flow had developed between the diffuser walls.

Researchers showed that, (Johnson and Moore, 1980; Moore et al., 1987) for a turbine cascade, a major contributor to loss production within the turbulent boundary layers and passage vortex is the conversion of mean kinetic energy to turbulent kinetic energy and hence to total pressure loss due to turbulent dissipation. Such a conversion process is only possible where shear is present in the mean flow, e.g. within the boundary layers or within the secondary flow regions associated with a passage vortex. Most turbomachines discharge a complex 3-d flow exhibiting several flow features which will ultimately result in turbulent dissipation and loss. The designers' problem is in identifying features which are the major contributors to the loss such that he can attempt to modify his design to reduce their effect.

The centrifugal compressor vaneless diffuser is a good example for the study of losses due to turbulent dissipation. The geometry is simple, but because the flow entering the diffuser is highly non-uniform with strong secondary flows, turbulent dissipation leads to relatively high losses. The purpose of this paper is to study the flow mechanisms which lead to the losses within a low speed centrifugal compressor vaneless diffuser.

2. Experimental procedure

A schematic of the low speed centrifugal compressor rig used in the study is shown in Fig. 1. The impeller was a De Havilland Ghost impeller, the geometry of which is given by Johnson and Moore (1983). In the current study, the original radial outlet section was replaced to provide a 30° backswept outlet angle as detailed

* Tel.: +90 346 2191339; fax: +90 346 219 11 75.
E-mail address: alipinarbasi@cumhuriyet.edu.tr

0142-727X/$ - see front matter © 2008 Elsevier Inc. All rights reserved.
doi:10.1016/j.ijheatfluidflow.2008.12.001

Nomenclature

A, B, c	King's law calibration coefficients
E	hot wire anemometer voltage
h, k	directional coefficients for hot wire
L	radial distance from impeller outlet
Q	non-dimensional turbulent kinetic energy
r, θ, z	cylindrical coordinate system
R_o	impeller outlet radius
R	radial coordinate
U_e	effective cooling velocity
U_T	peripheral blade velocity at the impeller outlet
u_θ, u_r, u_z	radial, tangential and axial mean velocity components
u'_θ, u'_r, u'_z	radial, tangential and axial r.m.s fluctuating velocity components
U_n, U_t, U_b	normal, tangential and binormal velocity components relative to the wire
Y	tangential coordinate in measurement plane
y_0	tangential distance between consecutive blade wakes
z	axial coordinate in measurement plane
z_0	axial diffuser width in measurement plane

in Fig. 2. The vaneless diffuser has straight walls and a constant cross sectional area. The geometry, operating conditions and measurement stations are summarized in Table 1 and details are given in Fig. 3.

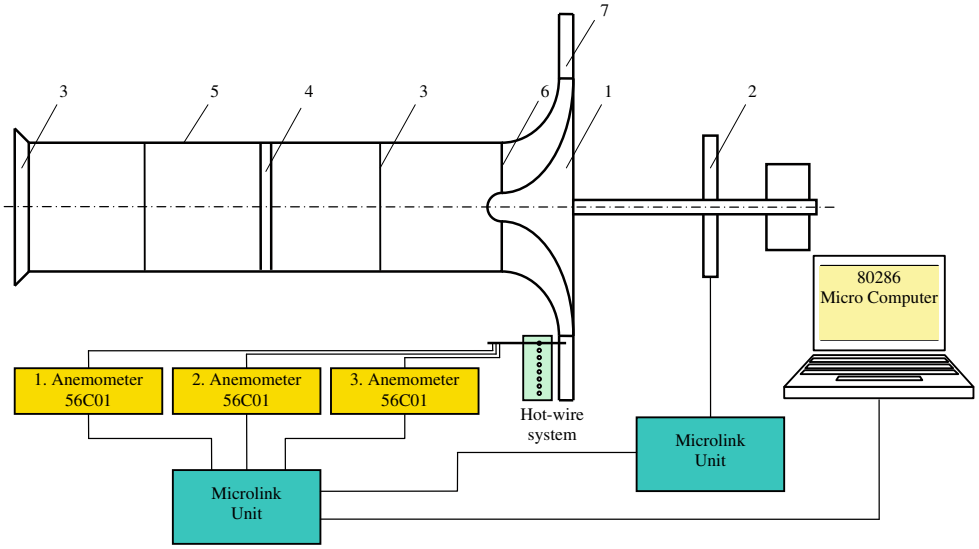

1-Impeller 2-Pulley Driven by motor 3-Screens 4-Honeycomp 5-Inlet Duck 6-Seal 7-Diffuser

Fig. 1. Schematic of centrifugal compressor test rig.

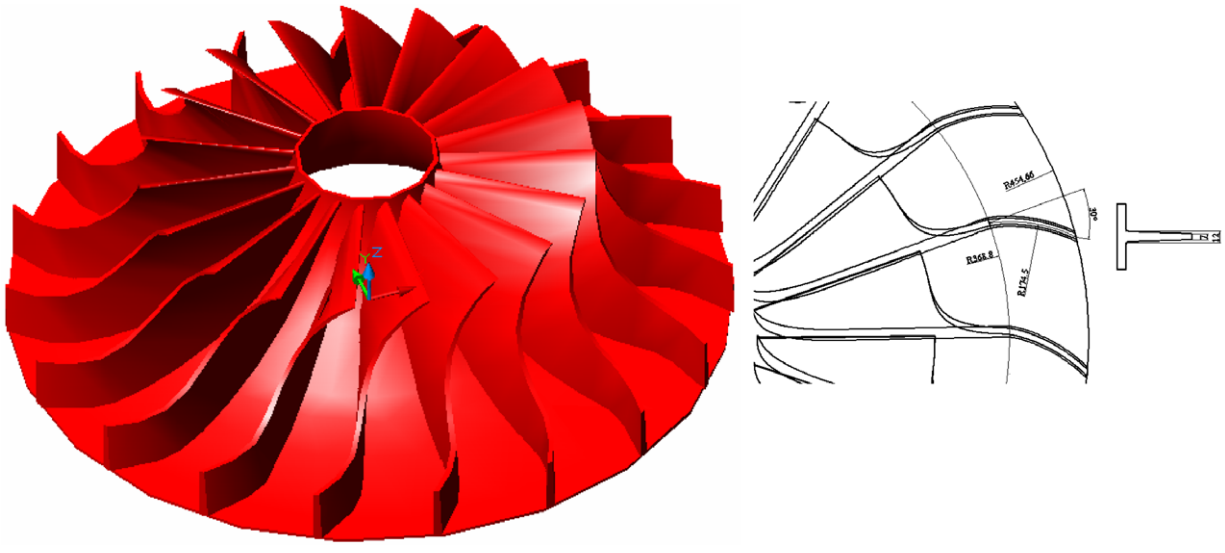

Fig. 2. Backswept impeller blade geometry.

Table 1
Impeller geometry and operating condition.

Impeller								
Inlet blade redius at the hub							R_h = 88.75 mm	
Inlet blade redius at the shroud							R_s = 283.75 mm	
Outlet radius							R_o = 454.6 mm	
Backswept blade angle							β = 30°	
Number of the blades							N = 19	
Outlet blade span							b = 72.3 mm	
Rotating speed							n = 500 rpm	
Mass flow rate (design point)							$\dot{m}$ = 0.1311 kg/s	
Measurement location								
Station	1	2	3	4	5	6	7	8
L/R_o	0.02	0.08	0.15	0.21	0.27	0.33	0.39	0.45

2.1. Instrumentation and measurement technique

A triple hot wire probe was used to measure the velocities within the diffuser at design flowrate level**.** A single wire (Dantec 55P11) was aligned circumferentially with a double wire (Dantec 55P61) arranged with each wire in the axial radial plane and at 45° to both the radial and axial directions. This mutually perpendicular arrangement of wires was therefore capable of resolving the axial, circumferential and radial velocity components and the directional sign of the axial component. It was assumed that the radial and circumferential components remained positive throughout the flow. There was no evidence in the results of either of these components reducing to zero and hence this assumption was justified. The hot wires were connected to three constant temperature hot wire anemometer bridges. The wires were then calibrated in two stages in a wind tunnel following the procedure of Jorgensen (1971) and detailed by Pinarbasi and Johnson (1994).

An optical shaft encoder provided a pulse for every 1/3° of impeller rotation. This was used to trigger the simultaneous sampling of the three anemometer voltages through a Microlink data acquisition unit. Readings from 57 measurement points spanning one of the 19 impeller passages were logged on each of 230 consecutive impeller revolutions. The triple wire sensor was traversed in the axial direction in order to provide a mesh of data points for each measurement plane.

The hot wire anemometer voltages are first converted to effective wire cooling velocities using King's law. According to King's Law, the voltage E is related to the effective cooling velocity U_e by the following relationship

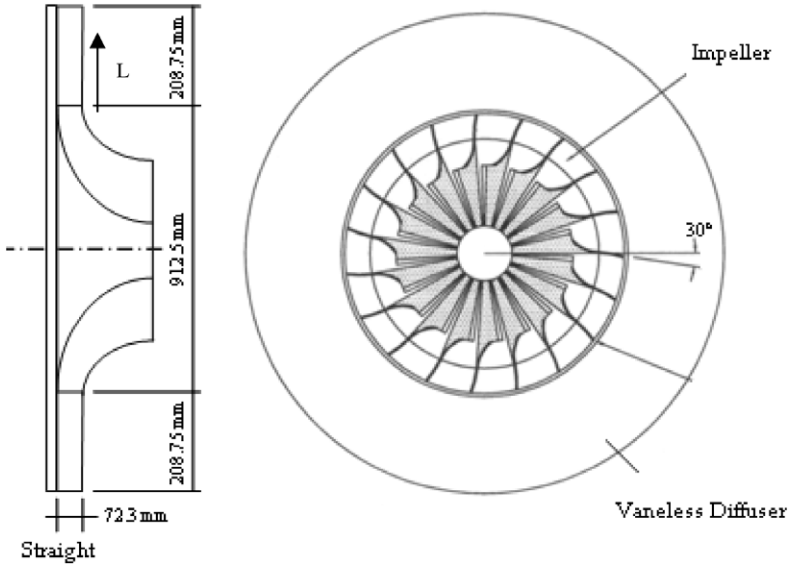

Fig. 3. Diffuser details.

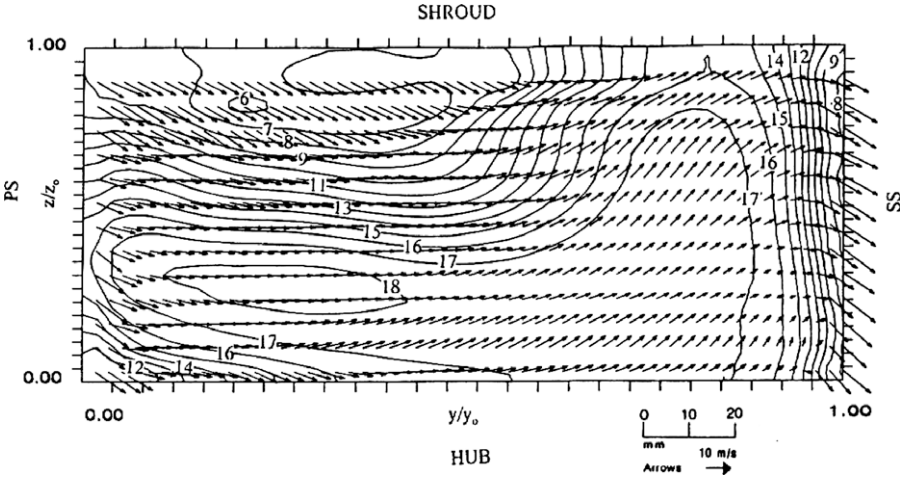

Fig. 4. Mean velocities at station 1.

$$E^2 = A + BU_e^c \quad (1)$$

where A represents the heat loss through natural convection and conduction along the prongs at zero velocity. The coefficients A, B and c are determined by calibration of the wire in a wind tunnel.

A careful study of the directional sensitivity of the wires was undertaken to determine the relationship between the three effective wire cooling velocities and the three mutually perpendicular velocity components. For each wire King's Law states that

$$U_e^2 = U_n^2 + KU_t^2 + HU_b^2 \quad (2)$$

where U_n, U_t and U_b are the normal, tangential and binormal velocity components relative to the wire. The coefficients H and K were

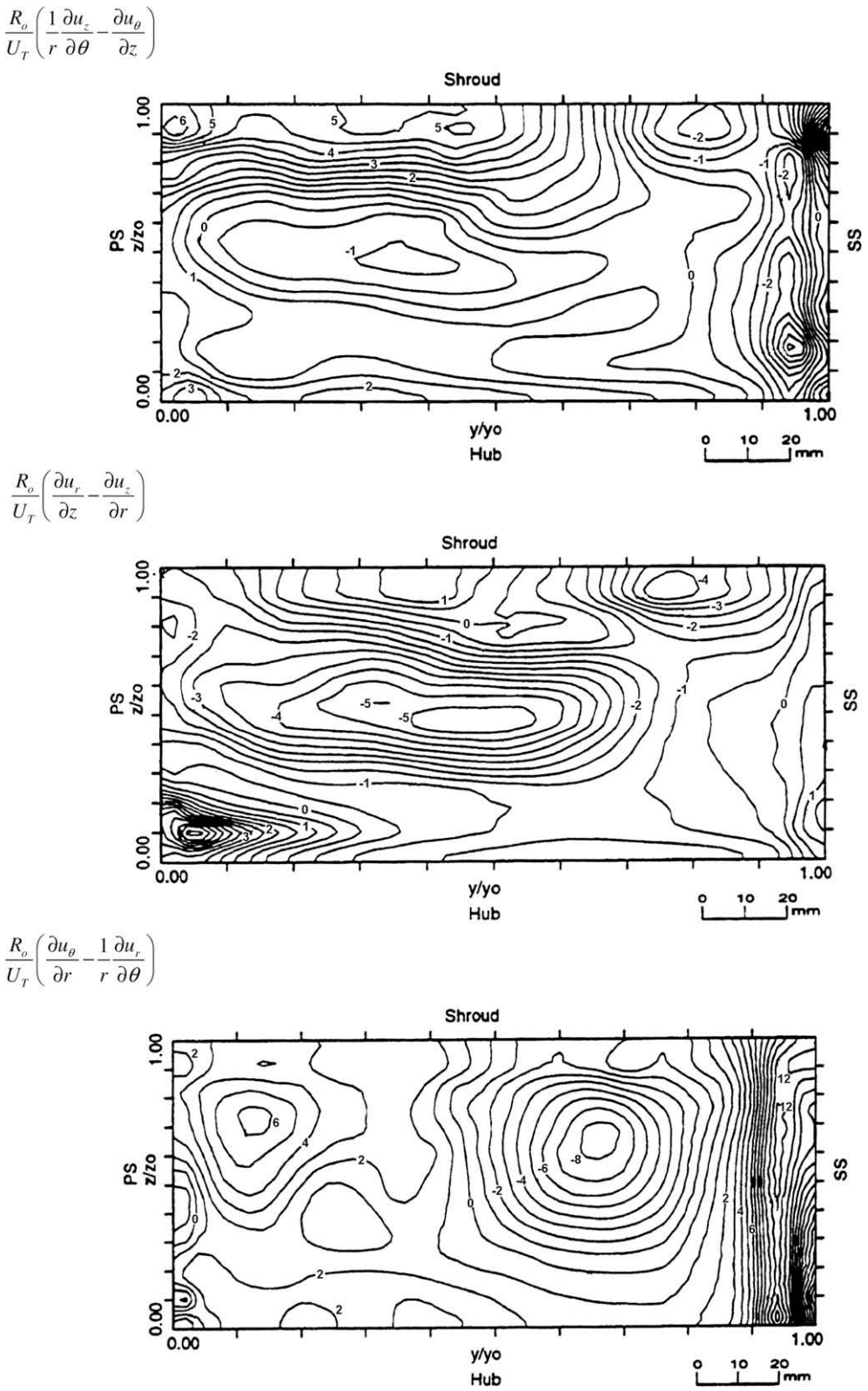

Fig. 5. Radial, tangential and axial components of dimensionless vorticity.

determined by varying the wire orientation at fixed wind tunnel speed. The probe was rotated through a range of ±50° yaw and 20° pitch angles. Following calibration, measurements were made at 14 axial measurement probe locations on diffuser inlet passage cross sections. At each position reading were taken on each of 230 shaft revolutions at 1/3° interval of shaft rotation spanning one impeller passage. The mesh of data points is thus $8 \times 14 \times 57$ in the radial, axial and tangential directions, respectively.

Statistical methods were used to determine the three mean velocity components, vorticity, turbulent kinetic energy, stress components and turbulence production terms from the instantaneous velocities obtained on the 230 consecutive impeller revolutions at each measurement point.

The error analysis presented by Pinarbasi (1995) shows that uncertainties in the mean velocity components, the turbulent kinetic energy and the Reynolds stress components were ±1 m/s, ±0.1% and ±0.05%, respectively. The errors that would occur in measurements were attributed to the assumption of the constant coefficients in Eqs. (1) and (2). For more information about the error analysis, the reader can refer Pinarbasi (1995).

3. Experimental results

Results will only be presented at station 1, although mean velocity results from stations 2 and 3 have been used to evaluate the radial gradients of mean velocity using finite difference techniques.

3.1. Mean velocities

The mean velocities measured at station 1, which is 9 mm downstream of the impeller blade trailing edge, are shown in Fig. 4. The contours represent the radial component whereas the remaining components in the axial and tangential directions are depicted by an arrow at each measurement point. The flow pattern is typical of the *'jet-wake'* discharge flow characteristic of centrifugal machines. The passage wake is located in the shroud/pressure side quarter of the passage with its core at $y/y_0 = 0.35$ with the jet filling most of the remaining three quarters of the passage cross section. The wakes from two consecutive impeller blades result in the low velocity bands on the pressure side ($y/y_0 = 0$) and suction side ($y/y_0 = 1$) of the passage.

Strong secondary flows exist in the blade wake region, but within the passage the cross velocity arrows depict an anticlockwise circulation of the bulk flow which is also typical of backswept centrifugal impellers (Krain, 1988). Shear within the flow resulting from the boundary layers, the blade wakes, the passage wake and the secondary flows will thus lead to the production of turbulence which will ultimately dissipate resulting in total pressure loss.

The regions in the flow of high shear can also be identified by considering the three components of vorticity. The vorticity is computed from the mean velocities using second order finite differences with an estimated accuracy of ±10%. Fig. 5 shows the radial component of vorticity associated with the secondary flows observed in Fig. 4. The vorticity is positive (anticlockwise) over the majority of the cross section with the highest values occurring in the passage wake core ($y/y_0 = 0.35$, $z/z_0 = 1$) and where the passage wake interacts with the blade wake on the shroud ($y/y_0 = 1$, $z/z_0 = 1$). Clockwise rotation is observed though on the suction side of the passage at $y/y_0 = 0.95$ due to shear between the secondary flow from shroud to hub within the blade wake and the secondary flow in the opposite direction associated with the passage vortex.

The axial component of vorticity shows very high levels in the blade wake, particularly on the suction side. High levels are also associated with the shear gradients at either side of the passage wake ($y/y_0 = 0.15$, $z/z_0 = 0.7$ and $y/y_0 = 0.7$, $z/z_0 = 0.7$). The tangential component of vorticity also shows high levels in the middle of the passage where high shear is present between jet and wake. However, the highest levels occur in the pressure side/hub corner within the thickened hub boundary layer observed in Fig. 4.

3.2. Turbulent kinetic energy

The turbulent kinetic energy

$$q = \frac{\sqrt{u_r'^2 + u_\theta'^2 + u_z'^2}}{U_T} \tag{3}$$

shown in Fig. 6 indicates peak levels of 7% within the blade wake and at the core of the passage wake. Significant levels are observed

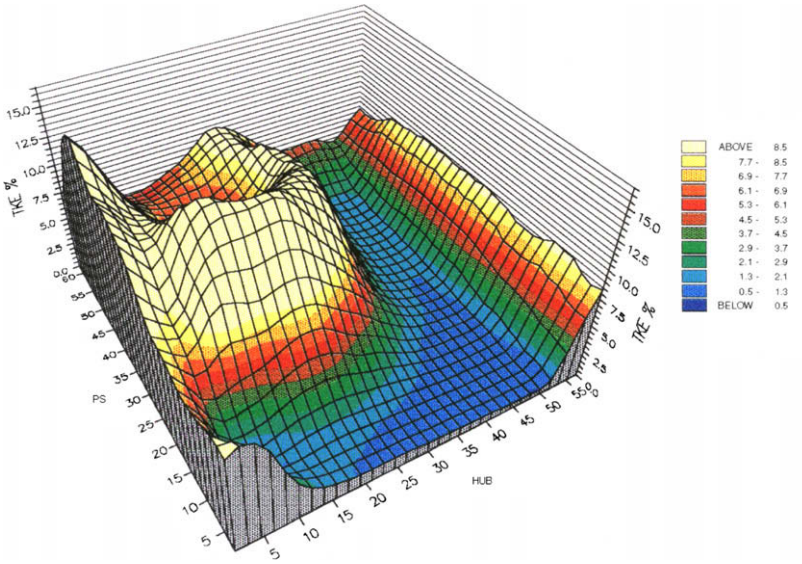

Fig. 6. Turbulent kinetic energy at station 1.

in the thickened hub boundary layer near the pressure side corner and also in the secondary flow interaction region close to the suction surface. The level within the jet is considerably lower between 0.5% and 1.5%.

3.3. Stress tensor

Anisotropic turbulence exists at inlet as demonstrated by the Reynolds stress components of the straight wall diffuser. The peak levels

$$\left(\frac{\overline{u_r' u_r'}}{U_T^2} - \frac{q^2}{3}\right) \Big/ \frac{q^2}{3}$$

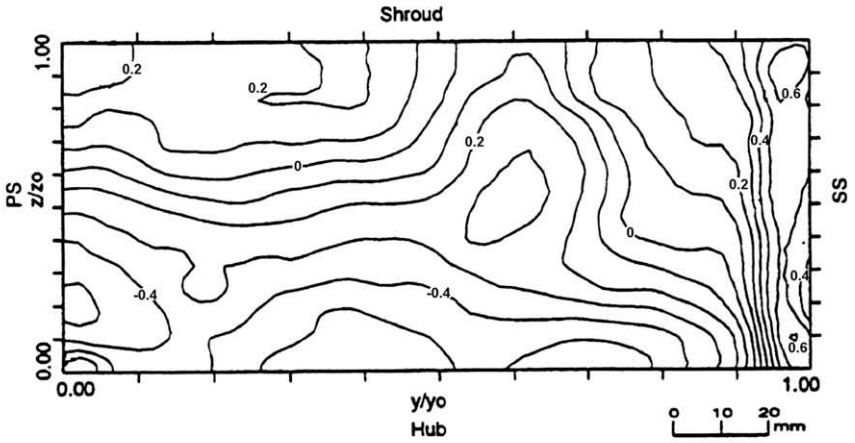

$$\left(\frac{\overline{u_\theta' u_\theta'}}{U_T^2} - \frac{q^2}{3}\right) \Big/ \frac{q^2}{3}$$

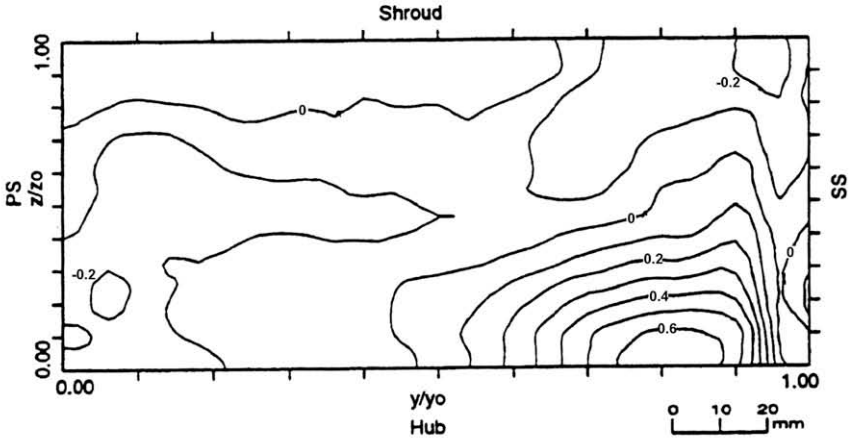

$$\left(\frac{\overline{u_z' u_z'}}{U_T^2} - \frac{q^2}{3}\right) \Big/ \frac{q^2}{3}$$

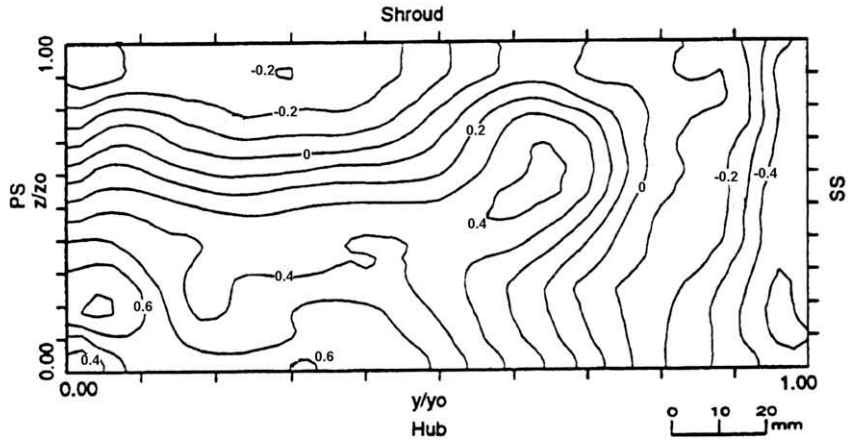

Fig. 7. Non-isotropy factors at station 1.

of Reynolds stress are due to the streamline curvature effect and also where the velocities are higher. The three direct stress and three shear stress terms in the stress tensor are shown in Figs. 7 and 8. The direct stresses are presented as non-isotropy factors. Thus negative values correspond to below average contributions from the direct stress to the turbulent kinetic energy and positive values to an above average contribution. Fig. 7 shows that the turbulence is highly non-isotropic within the blade wake, where the direct stresses are primarily in the radial and tangential directions. This might be expected since the vorticity (Fig. 5) is in the axial direction. Although other regions of high non-isotropicity exist, it is observed that the turbulence is essentially isotropic throughout the passage wake.

The three Reynolds stress components are presented in Fig. 8. These results are similar to measurements made downstream of

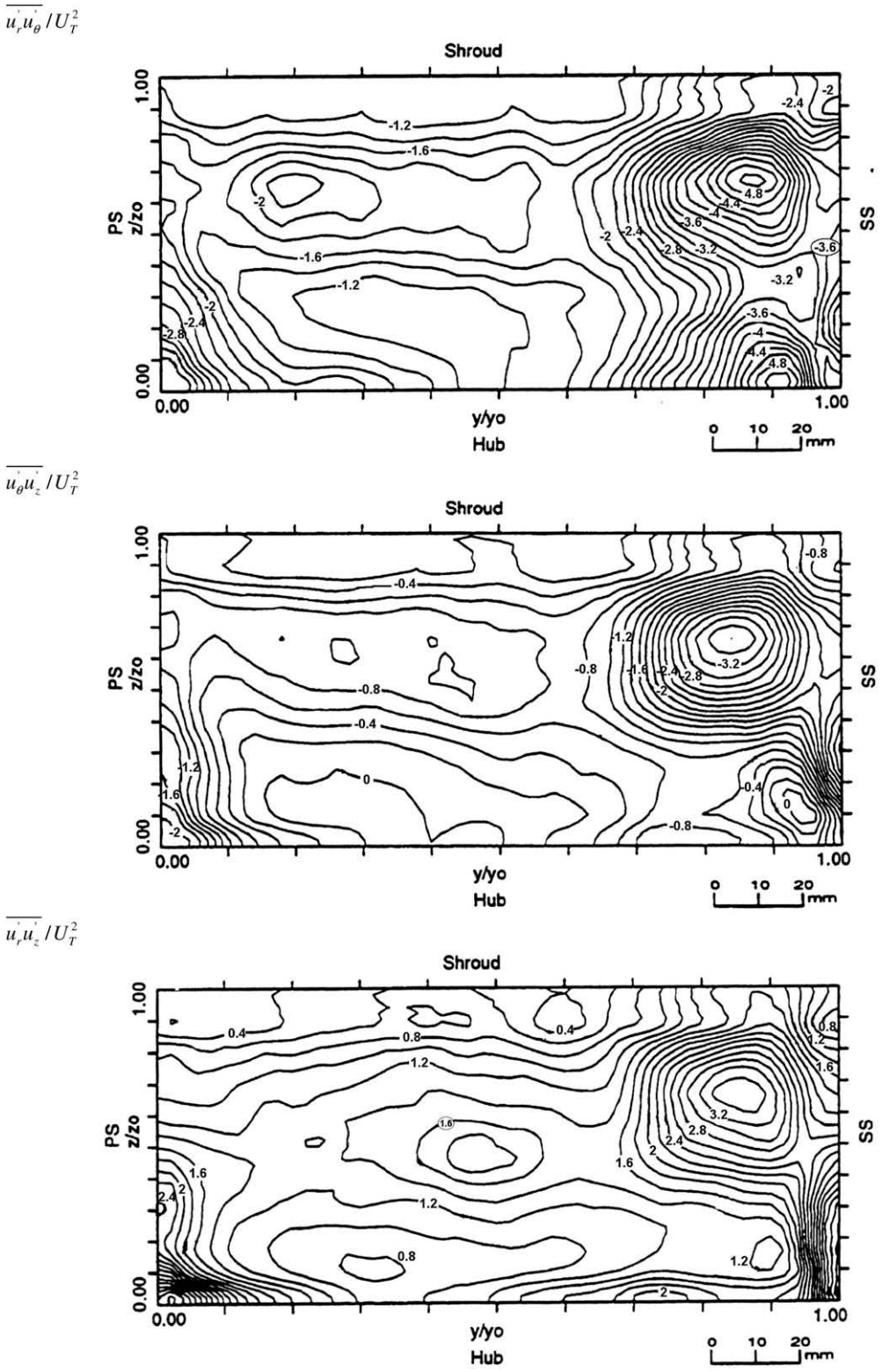

Fig. 8. Shear stress components at station 1.

a backward centrifugal impeller by Ubaldi et al. (1993). High levels are observed in the blade wake and also in the regions of high shear in the thickened hub boundary layer near the pressure surface corner and in the interaction region between the passage vortex and the secondary flow within the blade wake. There are thus some similarities with the corresponding components of vorticity in Fig. 5. The most significant difference is that the high levels of vorticity associated with the shear layers around the passage wake do not lead to significant levels of Reynolds stress. This identifies an important difference between the turbulence within the passage and blade wakes. The passage wake has its shear origins within the impeller and hence its shear layers are more fully developed

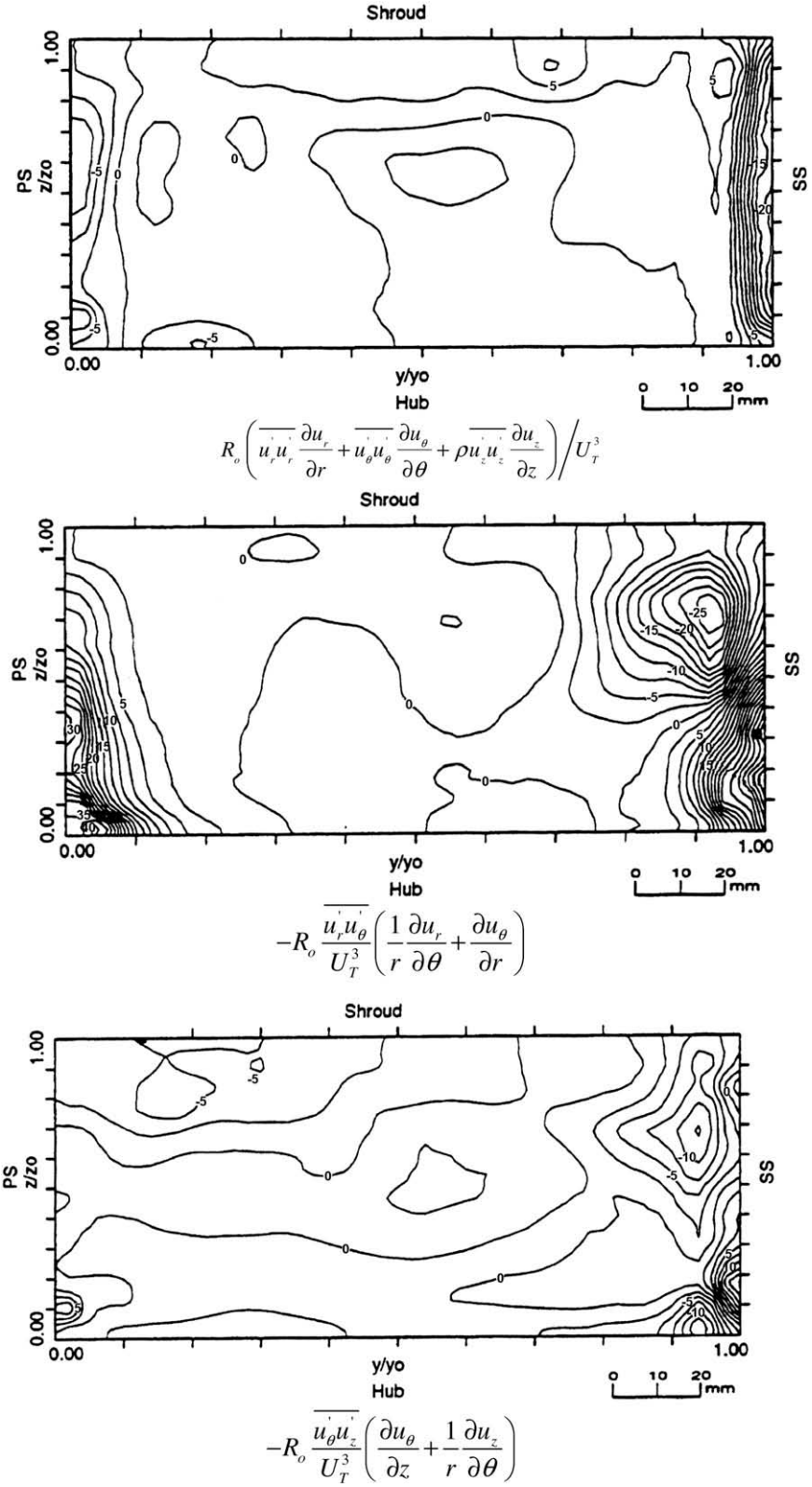

Fig. 9. Turbulence production term at station 1.

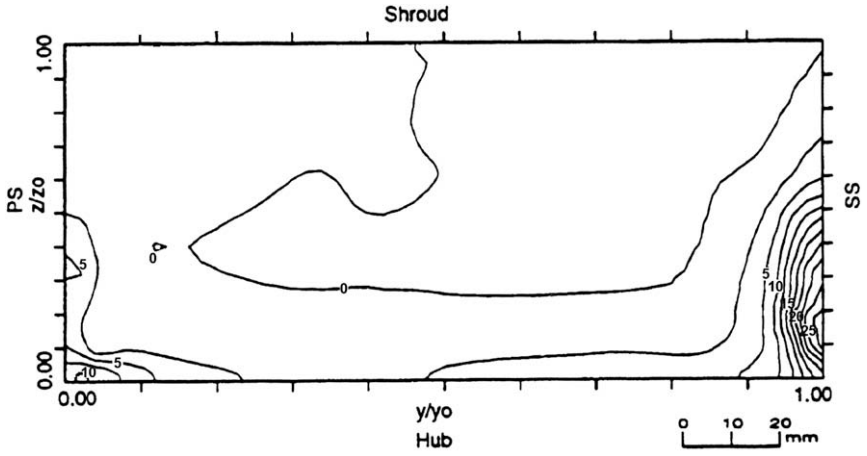

$$-R_o \frac{\overline{u_r' u_z'}}{U_T^3}\left(\frac{\partial u_r}{\partial z}+\frac{\partial u_z}{\partial r}\right)$$

Fig 9. *(continued)*

than those associated with the blade wakes which are only generated at the impeller exit. The author therefore believes that the high levels of turbulent kinetic energy within the passage wake (Fig. 6) are due to low frequency meandering in the passage wake position rather than high frequency turbulence. Hathaway et al. (1992) have also suggested that meandering in the passage wake position occurs within their low speed centrifugal compressor impeller. The wake position is sensitive to the impeller passage flow rate (Moore and Moore, 1983) and to the strength of the tip leakage jet (Farge et al., 1988) and hence relatively small variations in flow rate and blade loading will cause significant variations in the passage wake position.

3.4. Turbulence production

Reynolds (1895), in his famous paper which defined Reynolds stresses, derived an expression for turbulence production

$$-\begin{bmatrix} \rho\overline{u'u'}\frac{\partial u}{dx}+\rho\overline{u'v'}\frac{\partial u}{dy}+\rho\overline{u'w'}\frac{\partial u}{dz} \\ +\rho\overline{v'u'}\frac{\partial v}{dx}+\rho\overline{v'v'}\frac{\partial v}{dy}+\rho\overline{v'w'}\frac{\partial v}{dz} \\ +\rho\overline{w'u'}\frac{\partial w}{dx}+\rho\overline{w'v'}\frac{\partial w}{dy}+\rho\overline{w'w'}\frac{\partial w}{dz} \end{bmatrix} \tag{4}$$

This expression has recently been used by Moore and Moore (1995) and Moore et al. (1994) to determine the origins of the turbulence generated within the tip vortex of a turbine cascade.

Moore et al. (1994) grouped these nine terms into (using the current notation) a direct stress term

$$-\rho\overline{u_r'u_r'}\frac{\partial u_r}{\partial r}-\rho\frac{\overline{u_\theta'u_\theta'}}{r}\frac{\partial u_\theta}{\partial\theta}-\rho\overline{u_z'u_z'}\frac{\partial u_z}{\partial z} \tag{5}$$

and three shear stress terms,

$$\begin{aligned} &-\rho\overline{u_r'u_\theta'}\left(\frac{1}{r}\frac{\partial u_r}{\partial\theta}+\frac{\partial u_\theta}{\partial r}\right) \\ &-\rho\overline{u_\theta'u_z'}\left(\frac{\partial u_\theta}{\partial z}+\frac{1}{r}\frac{\partial u_z}{\partial\theta}\right) \\ &-\rho\overline{u_r'u_z'}\left(\frac{\partial u_r}{\partial z}+\frac{\partial u_z}{\partial r}\right) \end{aligned} \tag{6}$$

The peak of the these components are shown in Fig. 9 and contribute 22%, 39%, 22% and 17%, respectively, to the total turbulence production. The normal stress term contributes primarily to the turbulence production within the blade wake. The first of the shear stress terms is the strongest contributor to turbulence production within the blade wake although significant contributions are also made from the remaining shear stress terms. Fig. 9 also shows quite clearly how the first and third shear stress terms generate turbulence within regions of primary velocity shear in the blade wake and boundary layers whereas the middle term, which is only dependent on the secondary velocities u_θ and u_z, generates turbulence only in regions of secondary velocity shear. These results suggest that the blade wake is responsible for about three quarters of the turbulence production with most of the remainder coming from the secondary flows. It should be noted that the relative contributions to turbulence production will be dependent on the impeller flow. The strength of the secondary flows at the impeller exit and the thickness of the blade trailing edge will be of particular significance.

4. Conclusions

(1) Four regions of high shear rate are identified within the flow – within the blade wake, between the passage wake and jet, within the thickened hub boundary layer and between the blade wake secondary flow and passage vortex. Each of these regions is associated with high turbulent kinetic energy and with high levels in at least one component of vorticity.
(2) Significant Reynolds stresses are generated in all these regions except between the passage wake and jet. The author believes that these observations suggest that the passage wake is meandering in position.
(3) Enhanced levels of Reynolds stress appear to occur in regions where streamline curvature and strong velocity gradients would be due to frequency meandering of the wake position rather than high frequency turbulent mixing.
(4) The turbulence production terms show how most of the losses can be attributed to mixing out of the blade wakes. Significant losses do occur however in the suction side shroud corner region due to interaction of the secondary flow within the blade wake with the passage vortex and within the hub boundary layer. There is no evidence of significant turbulence production within the passage wake.
(5) If losses in centrifugal compressor diffuser flows are to be predicted accurately, the turbulence production terms within CFD codes need to be correctly modelled. The non-

isotropicity of the turbulence exhibited by the current results suggests that turbulence models which assume isotropicity (e.g. k–ε and Baldwin Lomax) are unlikely to be adequate for this purpose. It therefore follows that full Reynolds stress turbulence models will be required if reliable prediction of the details of turbulent production is to be achieved within diffuser flows.

References

Dean Jr., R.C., Senoo, Y., 1960. Rotating wakes in vaneless diffusers. ASME J. Basic Eng., 563–570.

Farge, T.Z., Johnson, M.W., 1992. Effect of flow rate on loss mechanisms in a backswept centrifugal impeller. J. Heat Fluid Flow 13 (2), 189–196.

Farge, T.Z., Johnson, M.W., Maksoud, T.M.A., 1988. Tip leakage in a centrifugal impeller. ASME Paper 88-GT-210.

Hagelstein, D., Hillewaert, K., Van den Braembussche, R.A., Engeda, A., Keiper, R., Rautenber, M., 2000. Experimental and numerical investigation of the flow in a centrifugal compressor volute. J. Turbomach. 122 (1), 22–31.

Hathaway, M.D., Chriss, R.M., Wood, J.R., Strazisar, A.J., 1992. Experimental and computation of the NASA low speed centrifugal compressor field. ASME Paper 92-GT-213.

Hillewaert, K., Van den Braembussche, RA., 1999. Numerical simulation of impeller–volute interaction in centrifugal compressors. J. Turbomach. 121 (3), 603–608.

Inoue, M., Cumpsty, N.A., 1984. Experimental study of the centrifugal impeller discharge flow in vaneless diffusers. ASME J. Eng. Gas Turbines Power 106, 455–467.

Johnson, M.W., Moore, J., 1980. The development of wake flow in a centrifugal compressor. ASME J. Eng. Power 102, 383–390.

Johnson, M.W., Moore, J., 1983. Influence of flow rate on the wake in a centrifugal impeller. ASME J. Eng. Power 105, 33–39.

Jorgensen, F.E., 1971. Directional sensitivity of wire and fibre film probes. DISA Information No. 11, p. 31–37.

Krain, H., 1988. Swirling impeller flow. ASME J. Turbomach. 110, 122–128.

Maksoud, T.M.A., Johnson, M.W., 1989. Stress tensor measurements within the vaneless diffuser of a centrifugal compressor. J. Mech. Eng. Sci. 203 (C1), 51–59.

Moore, J., Moore, J.G., 1983. Entropy production rates from viscous flow calculation, Part 1 – a turbulent boundary layer flow. ASME Paper 83-GT-70.

Moore, J., Moore, J.G., 1995. Osborne Reynolds: energy methods in transition and loss production: a Centennial perspective. ASME. J. Turbomach 117, 142–153.

Moore, J., Shaffer, D.M., Moore, J.G., 1987. Reynolds stresses and dissipation mechanisms downstream of a turbine cascade. ASME J. Turbomach. 109, 258–267.

Moore, J., Moore, J.G., Heckel, S.P., Ballesteros, R., 1994. Reynolds stresses and dissipation mechanisms in a turbine tip leakage vortex. ASME Paper 94-GT-267.

Pinarbasi, A., 1995. Flow investigation in centrifugal compressor vaneless and vaned diffuser. PhD. Thesis, University of Liverpool.

Pinarbasi, A., Johnson, M.W., 1994. Detailed flow measurements in a centrifugal compressor vaneless diffuser. ASME J. Turbomach. 116, 453–461.

Reynolds, O., 1895. On the dynamical theory of incompressible viscous fluids and the determination of the criteria. Philos. Trans. Roy. Soc. A 186, 123.

Senoo, Y., Ishida, M., 1975. Behaviour of severely asymmetric flow in a vaneless diffuser. ASME J. Eng. Power 97 (3), 375–387.

Shum, Y.K.P., Tan, C.S., Cumpsty, N.A., 2000. Impeller–diffuser interaction in a centrifugal compressor. J. Turbomach. 122, 777–786.

Ubaldi, M., Zunino, P., Cattanei, A., 1993. Relative flow and turbulence measurements downstream of a backward centrifugal impeller. ASME J. Turbomach. 115, 543–551.